# Terrestrial biodiversity threatened by increasing global aridity velocity under high-level warming

Hao Shi[a,b] , Hanqin Tian[a,1], Stefan Lange[c], Jia Yang[a,d], Shufen Pan[a] , Bojie Fu[b], and Christopher P. O. Reyer[c]

[a]International Center for Climate and Global Change Research, School of Forestry and Wildlife Sciences, Auburn University, Auburn, AL 36849; [b]State Key Laboratory of Urban and Regional Ecology, Research Center for Eco-Environmental Sciences, Chinese Academy of Sciences, Beijing 100085, China; [c]Potsdam Institute for Climate Impact Research, Member of the Leibniz Association, Potsdam 14412, Germany; and [d]Department of Forestry, Mississippi State University, Starkville, MI 39762

Global aridification is projected to intensify. Yet, our knowledge of its potential impacts on species ranges remains limited. Here, we investigate global aridity velocity and its overlap with three sectors (natural protected areas, agricultural areas, and urban areas) and terrestrial biodiversity in historical (1979 through 2016) and future periods (2050 through 2099), with and without considering vegetation physiological response to rising $CO_2$. Both agricultural and urban areas showed a mean drying velocity in history, although the concurrent global aridity velocity was on average +0.05/+0.20 km/yr$^{-1}$ (no $CO_2$ effects/with $CO_2$ effects; "+" denoting wetting). Moreover, in drylands, the shifts of vegetation greenness isolines were found to be significantly coupled with the tracks of aridity velocity. In the future, the aridity velocity in natural protected areas is projected to change from wetting to drying across RCP (representative concentration pathway) 2.6, RCP6.0, and RCP8.5 scenarios. When accounting for spatial distribution of terrestrial taxa (including plants, mammals, birds, and amphibians), the global aridity velocity would be -0.15/-0.02 km/yr$^{-1}$ ("-" denoting drying; historical), -0.12/-0.15 km/yr$^{-1}$ (RCP2.6), -0.36/-0.10 km/yr$^{-1}$ (RCP6.0), and -0.75/-0.29 km/yr$^{-1}$ (RCP8.5), with amphibians particularly negatively impacted. Under all scenarios, aridity velocity shows much higher multidirectionality than temperature velocity, which is mainly poleward. These results suggest that aridification risks may significantly influence the distribution of terrestrial species besides warming impacts and further impact the effectiveness of current protected areas in future, especially under RCP8.5, which best matches historical $CO_2$ emissions [C. R. Schwalm et al., Proc. Natl. Acad. Sci. U.S.A. 117, 19656–19657 (2020)].

terrestrial biodiversity | climate velocity | aridification | global warming

There is general agreement that climate warming will be one of the greatest threats to ecosystem functioning in multiple ways and have substantial impacts on agriculture and human health (1, 2). As a response to warming, precipitation will also increase but with large spatial heterogeneity (3). The reshuffling of temperature and precipitation will lead to a shift of current or emergence of new aridity regimes. These changes are predicted to result in complicated biological consequences as aridity plays an important role in controlling ecosystem dynamics and biogeochemical cycling (4–7). This is true even in humid regions, as the temporal distribution of water availability is usually not uniform, and species have adapted to high water availability. Take tropical ecosystems as an instance; even modest changes in dry-season length can increase tropical tree mortality (8), and longer dry seasons can change the population growth rates and structure of tropical bird communities (9). Persistent drying would degrade tropical forest canopies (10) and, furthermore, have detrimental effects on biodiversity (11), resulting in functional, taxonomic, and phylogenetic homogenization (12).

Many studies have reported warming impacts on species ranges (13, 14), such as their poleward and uphill shifts. Yet, how aridity changes will drive species shifts has not been well addressed. Moreover, most previous studies ignored species like different varieties of crops and urban trees in human-managed systems. To date, it is still a grand challenge to assess the shift rate of each major species in response to climate forcing, as species-specific migration models are usually built upon very limited observations in the current climate conditions (15, 16). Therefore, we use the generic but ecologically relevant local climate velocity to approximate species migration rates (14, 17), which, through merging spatial and temporal gradients, describes the moving speed and direction required by a point to maintain its current climate domain. A number of studies have shown a remarkable correlation between observed terrestrial or marine species shifts and the velocity of climate warming (18–20). Since ecosystems are individually or jointly controlled by temperature and water availability, it is expected that ecosystems will also be impacted by the aridity velocity (derived from aridity index, the ratio of precipitation over potential evapotranspiration [PET]).

In this study, we evaluate how aridity velocity changes from historical (1979 through 2016) to future periods, using the aridity index based on the Food and Agriculture Organization of the United Nations (FAO) reference crop PET model (AI_RC) and one of its variants considering vegetation physiological responses to elevated $CO_2$ (AI_$CO_2$) developed by Yang et al. (21) Following Loarie et al. (14) and Diffenbaugh and Field (13), we focus on a future period (2050 through 2099) under three Representative Concentration Pathways (RCP2.6, RCP6.0, and RCP8.5) rather than the whole century, as climate change is more linear within a limited time window, facilitating the assumption of linear trends in estimating climate velocity. Meanwhile, we also calculate

## Significance

Under climate change, a point on a map needs to move in some speed and direction to maintain its current climate niche. We calculated the speeds and directions of aridity shifts across the globe to approximate species migration in natural–human systems driven by changes in water availability. We found historically that the aridity shifts had driven migration of vegetation greenness isolines in multiple regions. Most importantly, global drying would be accelerated for terrestrial taxa without mitigation. This would leave some species unable to adapt quickly enough, especially amphibians, which will suffer the largest aridification speed against plants, birds, and mammals. These findings suggest strong climate mitigation actions are required for the benefit of both terrestrial biodiversity and human well-being.

the migration of isolines of vegetation greenness using satellite observations during 1982 through 2015 to compare with the concurrent aridity velocity. Furthermore, we stack the projected aridity velocity to the global distributions of terrestrial vertebrates and plants to identify areas and taxa of high aridification risks. Because aridity is a nonlinear function of multiple climatic variables that may have complex interactions, it is hypothesized that aridity velocity would show nonuniform change under different RCPs.

## Results

Our results show that during 1979 through 2016, aridity velocities based on AI_RC and AI_CO$_2$ showed minor difference in either speed or direction (Fig. 1 *A* and *B*). Aridity velocity exhibited wetting patterns in Sahel Africa, southwestern Africa, most parts of Asia, and Australia but drying patterns in most of North and South America, Europe, Middle East, and west Russia (Fig. 1 *A* and 1*B*). In contrast, the changes in the concurrent temperature velocity were more homogeneous (Fig. 1*C*). The directions of aridity and temperature velocities showed obvious differences that aridity velocity (for both AI_RC and AI_CO$_2$) was more multidirectional at the global scale (*SI Appendix*, Fig. S1 *A* and *B*), whereas temperature velocity was generally poleward (*SI Appendix*, Fig. S1*C*), but at the regional scale, aridity velocity showed one uniform direction in some areas, such as in central United States (eastward), Sahel Africa (northward), and northwestern Australia (southward, *SI Appendix*, Fig. S1 *A* and *B*). In future, the aridity velocity tends to be more southward and eastward (*SI Appendix*, Fig. S1). We also compared the aridity velocities (for AI_RC) derived from two different historical climate datasets, i.e., EWEMBI (E2OBS, WFDEI and ERAI data merged and bias-corrected for ISIMIP) and CRUNCEP (combination of atmospheric forcing datasets by the Climatic Research Unit and the National Centers for Environmental Prediction), and found they were generally consistent in the spatial patterns (*SI Appendix*, Fig. S2) and had comparable global mean aridity velocity (+0.05 km/yr$^{-1}$ versus +0.01 km/

yr$^{-1}$), with major differences located in east North America and east Australia (*SI Appendix*, Fig. S2).

Aridity velocities under RCP2.6 generally show a weaker magnitude than those in history, but there would be more areas with drying velocities in the Southern Hemisphere (Fig. 1 *D* and *E*). Particularly in Australia, the historical wetting velocities would turn to drying velocities (Fig. 1 *D* and *E*) directing to coastlines (*SI Appendix*, Fig. S1 *D* and *E*). Higher warming under RCP6.0 would greatly influence the spatial patterns of aridity velocities in the Northern Hemisphere (*SI Appendix*, Fig. S1 *G* and *H*). The most obvious changes occur in east North America, western Europe, and east Siberia with the sign of aridity velocity reversed (Fig. 1 *G* and *H*). Further warming under RCP8.5 results in similar spatial patterns of aridity velocities to those under RCP6.0 but with larger speeds, notably in North America, Europe, east Siberia, South America, and southern Africa (Fig. 1 *J* and *K*). Across all the three RCP scenarios, the largest uncertainty (in SD) of aridity velocity among different climate projections occurs in northern high latitudes, Amazon and Australia (*SI Appendix*, Fig. S4). The spatial patterns of uncertainty in future aridity velocity are similar to those of future temperature velocity (*SI Appendix*, Fig. S3), and both are related to topography (*SI Appendix*, Fig. S4 and Discussion S1).

To validate whether the estimated aridity velocities are indicative of vegetation shifts, we calculated isolines of multiyear mean annual vegetation greenness during 1982 through 1986 and 2011 through 2015, respectively, using the Advanced Very High Resolution Radiometer (AVHRR) Normalized Difference Vegetation Index (NDVI3g) version 1 dataset. Northern Australia and Sahel and southern Africa (Fig. 2) were particularly taken as examples, because ecosystems in these regions are water dominated and have relatively flat landscapes and low intensity of human activities, such as irrigation, grazing, wood harvest, and deforestation (*SI Appendix*, Figs. S5–S8), which are particularly beneficial for detecting long-term expansion or contraction of vegetation ranges induced by aridity changes. The migration distances (*SI Appendix*, Method S1) of NDVI isolines in the
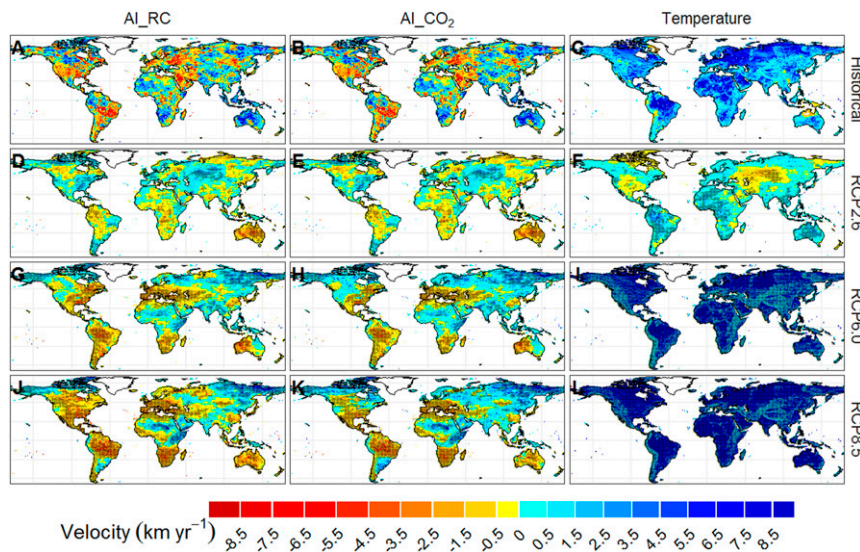


**Fig. 1.** Speed maps of historical and future aridity and temperature velocities. (*A, D, G, J*) Speed distribution of AI_RC-based aridity velocity in history, under RCP2.6, under RCP6.0, and under RCP8.5, respectively. (*B, E, H, K*) Speed distribution of AI_CO$_2$-based aridity velocity in history, under RCP2.6, under RCP6.0, and under RCP8.5, respectively. (*C, F, I, L*) Speed distribution of temperature velocity in history, under RCP2.6, under RCP6.0, and under RCP8.5, respectively. The negative sign of speed indicates drying/cooling, and the positive sign indicates wetting/warming. The future speed values are the ensemble mean of multiple models. Pixels in each speed map with values outside the 0.5 to 99.5% quantiles are removed. All velocities are calculated by using the spatial gradient during 1979 through 2016. Stippling indicates the agreement in the sign of estimated velocities under RCPs across at least seven of nine models (75% of models). AI_RC refers to the aridity index based on the FAO reference crop PET model and AI_CO$_2$ to one of its variants considering vegetation physiological responses to elevated CO$_2$.

Shi et al.
Terrestrial biodiversity threatened by increasing global aridity velocity under high-level
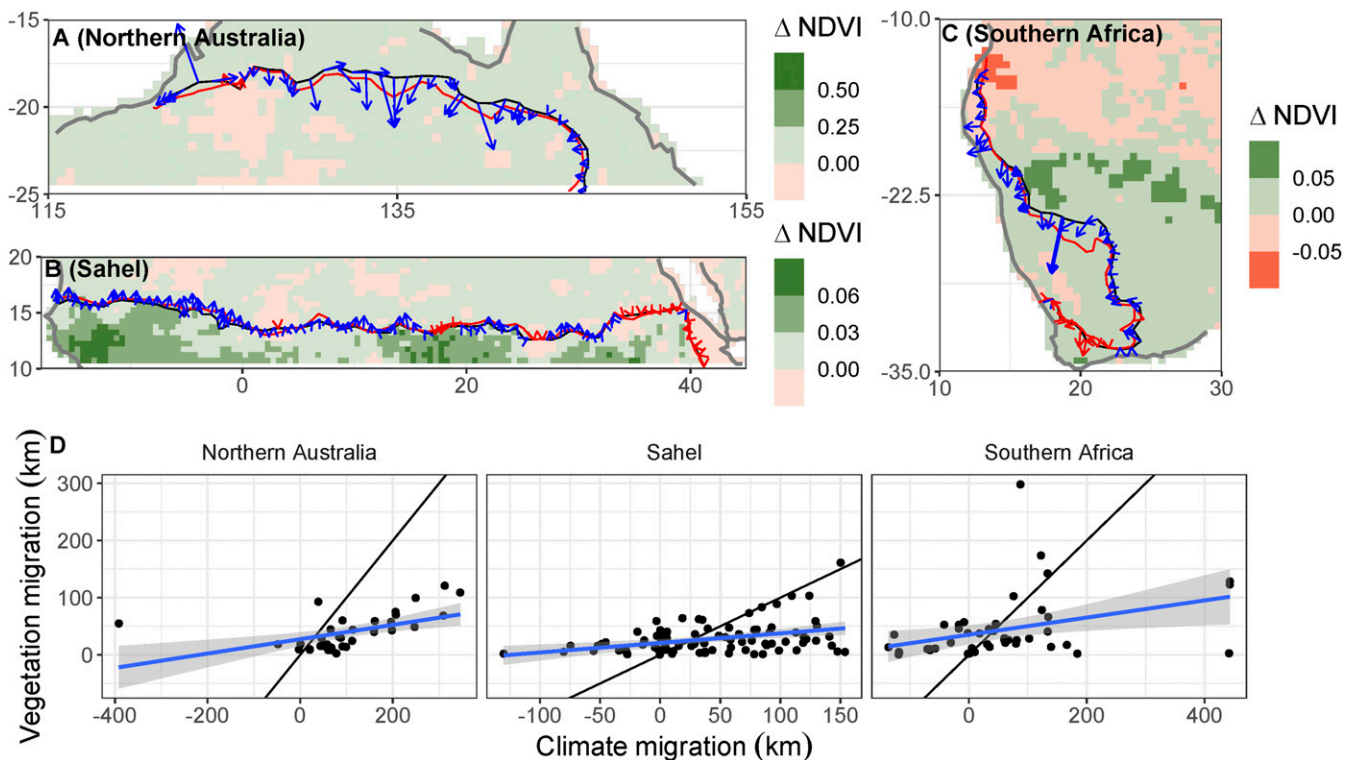
www.manaraa.com

**Fig. 2.** Coupling between aridity velocity (without considering CO₂ effects) and migration of NDVI isolines at multiple regions during 1982 through 2015. (*A*) The migration of NDVI isolines (NDVI = 0.30) in northern Australia during 1982 through 2015. (*B*) The migration of NDVI isolines (NDVI = 0.20) in Sahel during 1982 through 2015. (*C*) The migration of NDVI isolines (NDVI = 0.20) in southern Africa during 1982 through 2015. (*A–C*) The black and red lines denote NDVI isolines during 1982 through 1986 and during 2011 through 2015, respectively. The blue arrows indicate the directions of wetting velocity, and the red arrows indicate directions of drying velocity. The length of arrows represents the migration distances of aridity velocity. The aridity velocities are calculated based on the spatial gradient during 1982 through 2015. The pixel values indicate the differences between NDVI during 1982 through 1986 and that during 2011 through 2015. (*D*) Correlations between migration distances of points along the NDVI isolines and the climate migration distances derived using the aridity velocity of these points. The black line is 1:1 line. All correlations are statistically significant with $r = 0.52$ and $P < 0.002$, $r = 0.37$ and $P < 0.001$, and $r = 0.36$ and $P < 0.015$, respectively.

three regions were all significantly correlated with the concurrent aridity velocities (Fig. 2). Moreover, we also used the AVHRR vegetation continuous fields (VCF) data to investigate whether the isolines of herbaceous fractions migrated following aridity velocity. The results show that herbaceous VCF was significantly coupled with aridity velocity in both Sahel ($r = 0.35$ and $P < 0.001$; *SI Appendix*, Fig. S9B) and southern Africa ($r = 0.73$ and $P < 0.001$; *SI Appendix*, Fig. S9C), except in northern Australia. The reason lies in that the responses of vegetation greenness and vegetation composition to drying or wetting are not always synchronous. In northern Australia, as wetting during 1982 through 2015, NDVI generally increased, but herbaceous fraction decreased in a large extent (Fig. 2*A* and *SI Appendix*, Fig. S9A). Zhang et al. (22) also reported this phenomenon and found the altered rainfall climatology characterized by the increase of heavy rainfall favored woody vegetation in its competition with herbaceous vegetation.

Across the globe, aridity velocity basically obeys a Gaussian distribution, with the mean speed of AI_RC based aridity velocity from $+0.05$ km/yr$^{-1}$ in history changing to a drying speed of $-0.06$ km/yr$^{-1}$ under RCP2.6, $-0.19$ km/yr$^{-1}$ under RCP6.0 and $-0.42$ km/yr$^{-1}$ under RCP8.5, respectively (Fig. 3*A*). The corresponding global mean speed of AI_CO₂-based aridity velocity is $+0.20$ km/yr$^{-1}$, $-0.11$ km/yr$^{-1}$, $+0.13$ km/yr$^{-1}$, and $+0.15$ km/yr$^{-1}$, respectively (Fig. 3*E*). Beyond the global-average aridity velocities are their specific changes in protected areas, agricultural areas, and urban areas. Protected areas have covered ~4 to 25% of 14 major terrestrial biomes since 2009 and contain high

levels of endemism and small-ranged species. Thus, the changes of aridity velocity therein are more meaningful than the global average. Our analysis shows the aridity velocity in protected areas would change from historical $+0.22$ km/yr$^{-1}$/$+0.36$ km/yr$^{-1}$ (no CO₂ effects/with CO₂ effects) to $-0.72$ km/yr$^{-1}$/$-0.24$ km/yr$^{-1}$ under RCP8.5 (Fig. 3). The aridity velocity also manifests a significant change from historical $-0.56$ km/yr$^{-1}$/$-0.41$ km/yr$^{-1}$ to $-0.65$ km/yr$^{-1}$/$-0.13$ km/yr$^{-1}$ under RCP8.5 in agricultural areas (Fig. 3). In urban areas, the corresponding values are changing from $-0.66$ km/yr$^{-1}$/$-0.52$ km/yr$^{-1}$ to $-0.77$ km/yr$^{-1}$/$-0.24$ km/yr$^{-1}$ (Fig. 3). Of 18 socio-economic regions (*SI Appendix*, Fig. S10), protected areas in Brazil, southern Africa, Central America, and Oceania, agricultural areas in Brazil, Europe, southern Africa, and Central America, and urban areas in southern Africa, Europe, and Brazil would experience the largest drying velocity under RCP8.5 (*SI Appendix*, Fig. S11 and Discussion S2).

Since most wetting velocities occur in high latitudes under RCP6.0 and RCP8.5 (Fig. 1) while most terrestrial species live in low and high latitudes, it is necessary to consider the spatial pattern of terrestrial biodiversity to evaluate potential impacts of changing aridity velocity. When accounting for richness distribution of terrestrial taxa (including amphibians, birds, mammals, and plants), the global mean aridity velocity changes from historical $-0.15$ km/yr$^{-1}$ to $-0.12$ km/yr$^{-1}$, $-0.36$ km/yr$^{-1}$, and $-0.75$ km/yr$^{-1}$ based on AI_RC or from historical $-0.02$ km/yr$^{-1}$ to $-0.15$ km/yr$^{-1}$, $-0.10$ km/yr$^{-1}$, and $-0.29$ km/yr$^{-1}$ based on AI_CO₂, respectively, under the three RCPs. Across all scenarios, taxa in arid regions would experience the largest change in aridity velocity from
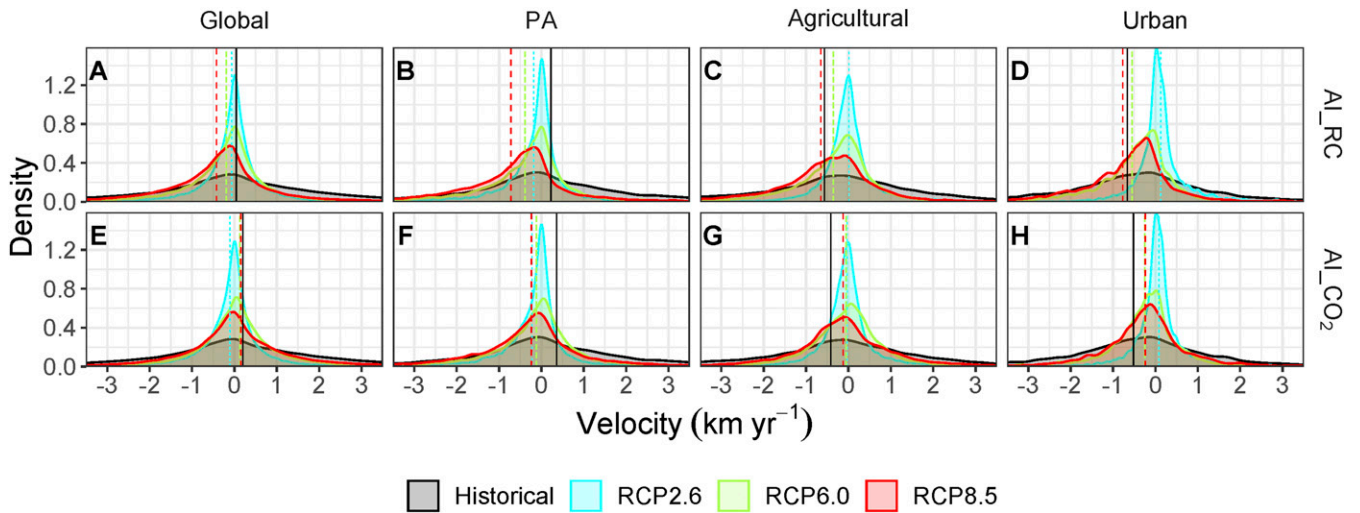
www.manaraa.com

**Fig. 3.** (*A–D*) Probability density distribution of speeds of AI_RC-based aridity velocity for the globe, protected areas (PA), agricultural areas, and urban areas. (*E–H*) Probability density distribution of speeds of AI_CO$_2$-based aridity velocity for the globe, protected areas, agricultural areas, and urban areas. Vertical lines indicate the global mean speeds of aridity velocity under different scenarios. In each land use type, the two-sample Student's *t* test is conducted for aridity velocities under different scenarios, and the results show they are all significantly different ($P < 0.001$). AI_RC refers to the aridity index based on the FAO reference crop PET model and AI_CO$_2$ to one of its variants considering vegetation physiological responses to elevated CO$_2$.

historical wetting to future drying (Fig. 4). Taxa in humid regions, which have the highest species richness, would experience the largest drying velocities under RCP8.5 (Fig. 4). Of all taxa, amphibians are projected to be most negatively impacted, particularly those in semiarid, semihumid, and humid regions under RCP8.5, which tracks closely cumulative CO$_2$ emissions until now (23).

## Discussion

The selected dryness metric is of central importance for aridity projection. AI_RC is questioned about overestimation of future dryness, as it lacks a description of vegetation physiological response to increasing CO$_2$ (24, 25). AI_CO$_2$ could reproduce CMIP5 projected runoff using the offline Budyko model over most of the globe through water-saving effects of elevated CO$_2$ (21). However, it must be noted that such water-saving effects

are not always persistent. For example, Ukkola et al. (26) reported that elevated CO$_2$ leads to vegetation greening (through CO$_2$ fertilization effects) and more water consumption in subhumid and semiarid basins but nonsignificant changes in NDVI and reductions in evapotranspiration in wet and arid basins across Australia during 1982 through 2010. Shimono et al. (27) also found that canopy evapotranspiration rate showed much lower responsiveness than stomatal conductance to open-air CO$_2$ elevation in rice. These observations mean that our original AI_RC formulation is still a reasonable approach in reflecting aridity changes even in a world of increasing CO$_2$ concentration. Therefore, AI_RC and AI_CO$_2$ are simultaneously used in this study to represent a spectrum of possible dryness change in future.

Before this effort, little research has focused on the impacts of water availability on species shifts except few examples (2, 28).
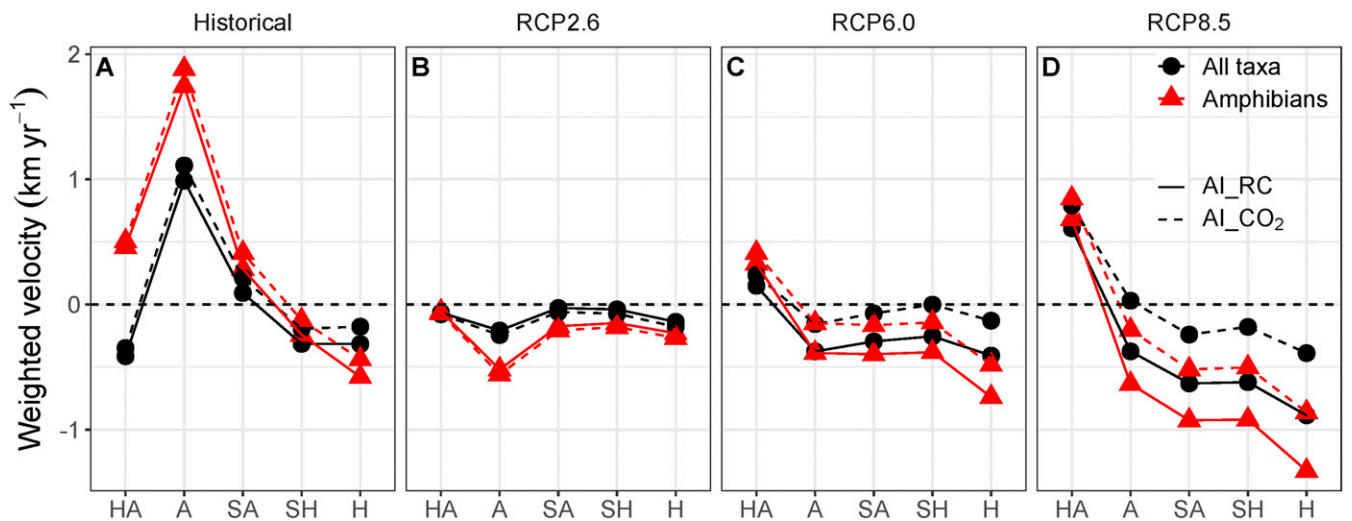


**Fig. 4.** Aridity velocities for all taxa (amphibians, birds, mammals, and plants) and amphibians under different scenarios. (*A–D*) The global mean speeds of aridity velocity based on AI_RC or AI_CO$_2$ for all taxa and amphibians in history, under RCP2.6, under RCP6.0, and under RCP8.5, respectively. The mean speed of aridity velocity for each taxon is weighted by grid area and species richness, in hyper-arid (HA), arid (A), semiarid (SA), subhumid (SH), and humid (H) regions. AI_RC refers to the aridity index based on the FAO reference crop PET model and AI_CO$_2$ to one of its variants considering vegetation physiological responses to elevated CO$_2$.

Shi et al.
Terrestrial biodiversity threatened by increasing global aridity velocity under high-level

www.manaraa.com

However, these exceptional studies still used precipitation to indicate water availability, which is projected to have an increasing trend opposite to aridity (*SI Appendix*, Fig. S12). Therefore, based on temperature only or even taking precipitation into account, when assessing threats of climate change to species shifts and the associated complexity, previous estimates could be underestimated. From this perspective, our results can provide complemental references for guiding allocation of limited conservation and adaptation resources.

For nature conservation, our estimated aridity velocity can help identify priority regions where species shifts are influenced by water availability, particularly at the leading edges of species range and for narrow-ranged species (15). In the identified hotspot areas, conservation actions may focus on monitoring of immigration or emigration of species and devote to mitigating other disturbances to aid indigenous species to adapt (15). A more specific example is that Malhi et al. (29) recommended to keep the core northwest Amazon intact as a biological refuge as it hosts the highest biodiversity and was expected to be the most resistant to climate drying in Amazon based on previous mid-range (A1B) emission scenarios. Our analysis, however, shows that the northwest Amazon is also projected to experience considerable drying under high-emission scenarios (Fig. 1), implying the imperative requirement for conservation actions to mitigate negative impacts of other factors in this area, such as reducing deforestation and controlling fires. Moreover, our results show that along coastal areas, aridity velocities may point to coastlines (e.g., Australia; *SI Appendix*, Fig. S1), which means many coastal niches could not find their climate analogs due to the ocean barrier. In addition, our methodology and results can help the design of protected-area networks and ecological corridors to connect large nature reserves across a continent. An excellent effort has been conducted in informing the design of the North American protected-area network (28). Batllori et al. (28) found that the majority of protected areas in North America might be exposed to high climate velocity and that the nearest climatic analogs are outside the current network of protected areas. Thus, they suggest that the conservation plan needs to take advantage of these unprotected climate refuges and avoid additional threats there beyond climate change.

Under all the three RCPs, some regions are projected to experience large aridification risks for crop species and food production, particularly in rain-fed areas like southern Africa and Brazil (*SI Appendix*, Fig. S13). Unfortunately, there has been much less research on migration of crop species, pasture, weeds, insects, etc. in responding to climate velocity. However, limited evidence shows that crop wild relatives could lose up to 91% of their distribution range in protected areas even with full dispersal under RCP8.5, which is 50% higher than that under RCP2.6 (30). Yield loss risk for four major crops (wheat, maize, rice, and soybeans) has also been reported across moderate to exceptional drought conditions, particularly in the United States, and it could be amplified by high temperature (31). A very recent study (32) also shows that changes in growing season temperature had driven migration of the harvested areas of rain-fed maize, wheat, rice, and soybean during 1973 through 2012. For species that are highly sensitive to climate change, the situation could be more severe. Take coffee for instance; its distribution area is predicted to decrease by about 50% across RCPs, and the new suitable habitats are far from the current plantation locations and currently occupied by forests (33). In addition, insects like locusts generally thrive in warm and dry conditions (34), and their dispersal-tracking aridity velocity will no doubt deteriorate food production. Therefore, as population increases, this might drive agricultural areas, irrigated fraction, or fertilizer application to increase to compensate for yield loss, in which case, securing food supply would inevitably conflict with the exacerbated aridity velocity predicted here and the increase of environmental externalities of crop production. To cope with this situation, crop drought traits and planting structure should be improved.

The drying velocities in urban areas (e.g., in Central America and Europe; *SI Appendix*, Fig. S11) could greatly influence plants, animals, and human health there. Since urban landscapes are usually highly fragmented, urban trees or forests are unlikely to escape from increased aridity through spatial shifts. Those tree species that are not suited to low water availability would have to be substituted by drought-tolerant species or irrigated more often, which will increase maintenance cost. Animals that depend on original trees or forests may suffer from water scarcity and loss of feeding source or shelters, and it is difficult for them to cross the urban barrier to migrate elsewhere. The possible decreased benefits provided by urban trees or forests, such as aesthetic value, tree shade, and air and water quality are associated with health problems (35–37). The efforts for enabling urban areas to adapt to the drying aridity velocity may involve high cost (e.g., infrastructure upgrade fees).

It is important to note that climate velocity has its own caveats. Brito-Morales et al. (15) summarized that climate velocity does not include biological information and may be misleading due to its fractional nature (i.e., ratio of a temporal trend over a spatial gradient). In our analysis, we also noticed that there existed some aridity velocities of abnormally large magnitudes compared to their neighboring counterparts (Fig. 2), and the migration of vegetation herbaceous fraction does not always track climate velocity (*SI Appendix*, Fig. S9A). Therefore, interpretation of changes in climate velocity and their impacts on biodiversity needs carefulness and a full consideration of the exposure, sensitivity, and vulnerability of individual species to climate change, together with their adaptive capacities (38). However, the magnitude and direction of climate velocity are still indicative in reflecting expected shifts of species ranges.

The spatial and temporal resolutions used in this analysis are also a potential source of uncertainty in estimating aridity velocity and its impacts on biodiversity. The half-degree climate data does not capture fine-scale topographic differences in climate and may underestimate climate heterogeneity, especially for urban or mountain areas. Therefore, our results may underestimate drying velocity in urban areas, as cities usually have higher temperature than neighboring areas due to the heat island effect. Meanwhile, the annual time step can obscure the signal of intra-annual variations in water availability, which may have considerable impacts on changes in ecosystem production and composition (8, 9). However, urban extent data and parameters and climate data at the half-degree or similar resolutions have been employed to examine interaction between urban expansion and climate warming (39–41), providing a certain confidence for employing climate data of the half-degree resolution. Moreover, consideration of long-term changes in aridity velocity of different seasons would be much more complex as different species or biological processes have different matching temporal windows (15). Therefore, for this study, we still focus on the annual changes in aridity velocity to keep it simple and leave seasonal climate velocity in future research, which could be another great story to explore.

## Materials and Methods

**Aridity Index.** We used the aridity index, the ratio of precipitation (mm yr$^{-1}$) to PET (mm yr$^{-1}$), to indicate aridity. PET is estimated through the FAO reference method (42; PET_RC) and one of its variants considering surface response to elevated $CO_2$ (22; PET_CO$_2$), which are parameterized, respectively, as

$$PET\_RC = \frac{0.408\Delta R_n^* + \gamma \frac{900}{T+273} uD}{\Delta + \gamma(1 + 0.34u)}, \quad [1]$$

$$PET\_CO_2 = \frac{0.408\Delta R_n^* + \gamma \frac{900}{T+273} uD}{\Delta + \gamma(1 + u(0.34 + 2.4 \times 10^{-4}([CO_2] - 300)))}, \quad [2]$$

where $\Delta$ (Pa K$^{-1}$) is the gradient of saturation vapor pressure against temperature, $R_n^*$ (MJ · m$^{-2}$ · d$^{-1}$) is the surface available net radiation, $\gamma$ (Pa · K$^{-1}$) is the psychrometric constant, $T$ (°C) is the air temperature at 2 m height, $D$

Shi et al.
Terrestrial biodiversity threatened by increasing global aridity velocity under high-level warming

PNAS | 5 of 7
https://doi.org/10.1073/pnas.2015552118

(Pa) is air vapor pressure deficit, $u$ (m $\cdot$ s$^{-1}$) is the wind speed at 2 m height, and [CO$_2$] is the atmospheric CO$_2$ concentration. These PET models take into account changes in available energy, atmospheric humidity, and wind speed and thus can give a more realistic estimation of PET than those methods only considering changes in temperature. During 1979 through 2016, the daily EWEMBI (40) (EartH2Observe, WATer and global CHange Forcing Data methodology applied to ERA-Interim data, and ERA-Interim data, merged and bias-corrected for the Inter-Sectoral Impact Model Intercomparison Project) and CRUNCEP version 8.0 datasets (both at a 0.5° resolution), including surface air temperature, precipitation, surface wind speed, atmospheric pressure, specific humidity, and downward shortwave radiation, were used to estimate daily PET, which then was aggregated to the annual time-scale to derive annual aridity index. For the future period, according to the RCP and daily data availability, we used outputs of nine global climate models, including the Commonwealth Scientific and Industrial Research Organization Mark 3.6.0 (CSIRO-Mk3.6.0), the Coupled Climate Model version 3 of the Geophysical Fluid Dynamics Laboratory (GFDL-CM3), the Earth System Model of the Geophysical Fluid Dynamics Laboratory (Modular Ocean Model version 4.1; GFDL-ESM2M), the Hadley Center Global Environment Model version 2 Earth System (HadGEM2-ES), the Earth System Model of the Institut Pierre Simon Laplace: Low Resolution (IPSL-CM5A-LR), the Model for Interdisciplinary Research on Climate version 5 (MIROC5), the atmospheric chemistry coupled version of the Earth System Model of MIROC (MIROC-ESM-CHEM), the Meteorological Research Institute Climate General Circulation Model 3 (MRI-CGCM3), and the Norwegian Climate Center's Earth System Model (NorESM1-M) to derive aridity index under RCP2.6, RCP6.0, and RCP8.5. These models can well represent the CMIP5 ensemble in terms of equilibrium climate sensitivity (3.55 °C versus 3.22 °C) and transient climate response (1.81 °C versus 1.84 °C; *SI Appendix*, Fig. S14). The climate projections have been bias-corrected at a daily timestep and downscaled referring to EWEMBI (https://doi.org/10.5194/gmd-10-4321-2017 and https://doi.org/10.5194/esd-9-627-2018). The annul aridity velocities of each of the nine models and the ensemble mean were adopted to represent the future aridity velocity under the three RCP scenarios and the corresponding SD.

**Aridity Velocity.** The local climate velocity approach (14) was used to calculate the moving speed and direction of aridity. Originally, the approach was introduced to estimate the local migration velocity of species to maintain their favorable temperatures as global warming shifts temperature isolines in space. Here, we apply the approach to both AI_RC and AI_CO$_2$ instead of to temperature. Specifically, climate velocity is calculated as $\frac{Temporalslope}{Spatialgradient}$. The temporal slope is derived by linearly regressing the annual time series in a grid cell. The spatial gradient is determined from a 3 × 3 window of mean climate during 1979 through 2016 using the cell-neighborhood method. The direction of climate velocity depends on both the sign of the temporal slope and the direction of the spatial gradient. The value of a velocity direction ranges from 0° to 360°, with 180° toward the straight south. Assuming the aridity velocity has a positive value of 1 km/yr$^{-1}$ and a spatial gradient direction of 90° during 2017 through 2050 and the reference mean climate is calculated from 1979 to 2016, the mean aridity in a specific grid cell during 1979 through 2016 could be found 33 km to the east by the year 2050, during which it has a drier climate than the grid during 1979 through 2016. In our analysis, the reference period was set to 1979 through 2016 to calculate the climatology of aridity index to derive the spatial gradient.

**Land Use, Region Classification, Vegetation Greenness, Herbaceous Cover Fraction, and Biodiversity Richness.** The protected areas (*SI Appendix*, Fig. S8) were compiled from the World Database on Protected Areas (WDPA, https://protectedplanet.net/), April 2019. The WDPA is the most comprehensive database of terrestrial and marine protected areas, jointly developed by the United Nations Environment and the International Union for Conservation of Nature. There are now over 220,000 protected areas, and only terrestrial ones are used here. The agricultural areas (including crops and pastures), urban areas, and irrigation fractions in 2018 (*SI Appendix*, Fig. S13) were from the Land-Use Harmonization Version 2h (LUH2, http://luh.umd.edu) data, which has a spatial resolution of 0.25° × 0.25° and an annual time step. The region classification is shown in *SI Appendix*, Fig. S10. The AVHRR GIMMS (Global Inventory Monitoring and Modeling System) NDVI data (NDVI3g version 1) in 1982 through 1986 and 2011 through 2015 was resampled from 1 km to 0.5° to show the spatial shifts of vegetation greenness isolines. The AVHRR VCF data (https://lpdaac.usgs.gov/products/vcf5kyrv001/) was also resampled from 0.05° to 0.5° to identify the spatial shifts of herbaceous fraction isolines. The plant biodiversity data were developed by combining spatially explicit models and estimates for native species loss and gains (43) and was achieved at https://ecotope.org/anthromes/biodiversity/plants/data/. The richness data for amphibians, birds, and mammals were mapped based on >21,000 species and at a spatial grain of 10 × 10 km (44) and available at https://biodiversitymapping.org/.

**Data Availability.** Climate data have been deposited in the ISIMIP data portal (https://doi.org/10.5880/pik.2019.004, https://doi.org/10.5880/PIK.2019.012). All other study data are included in the article and/or *SI Appendix*. Previously published data were used for this work (LUH2 [https://luh.umd.edu/data.shtml]: G. C. Hurtt et al., Harmonization of global land use change and management for the period 850–2100 [LUH2] for CMIP6. Geosci. Model Dev. 13, 5425–5464 [2020]. NDVI data [https://doi.org/10.3390/rs6086929]: J. E. Pinzon, C. J. Tucker, A nonstationary 1981–2012 AVHRR NDVI3g time series. Remote sensing 6, 6929–6960 [2014]. VCF data: https://lpdaac.usgs.gov/products/vcf5kyrv001/. Biodiversity data [https://biodiversitymapping.org/]: E. C. Ellis, E. C. Antill, H. Kreft, All Is Not Loss: Plant Biodiversity in the Anthropocene. PLOS ONE 7, e30535 [2012]. Protected areas data: the United Nations Environment Programme World Conservation Monitoring Centre [UNEP-WCMC] and the International Union for Conservation of Nature [IUCN] [2019], Protected Planet: Protected Areas [WDPA], April 2019, Cambridge, UK: UNEP-WCMC and IUCN. Available at: http://www.protectedplanet.net). The CRUNCEP data are freely available at https://vesg.ipsl.upmc.fr/thredds/catalog/work/p529viov/cruncep/V8_1901_2016/catalog.html. The bias-corrected GCMs outputs can be accessed from ISIMIP data portal (https://www.isimip.org/) upon request.

1. N. S. Diffenbaugh, D. L. Swain, D. Touma, Anthropogenic warming has increased drought risk in California. *Proc. Natl. Acad. Sci. U.S.A.* **112**, 3931–3936 (2015).
2. J. VanDerWal et al., Focus on poleward shifts in species distribution underestimates the fingerprint of climate change. *Nat. Clim. Chang.* **3**, 239 (2012).
3. A. G. Pendergrass, D. L. Hartmann, The atmospheric energy constraint on global-mean precipitation change. *J. Clim.* **27**, 757–768 (2014).
4. J. Bai et al., Satellite-observed vegetation stability in response to changes in climate and total water storage in Central Asia. *Sci. Total Environ.* **659**, 862–871 (2019).
5. M. Delgado-Baquerizo et al., Decoupling of soil nutrient cycles as a function of aridity in global drylands. *Nature* **502**, 672–676 (2013).
6. C. Wang et al., Aridity threshold in controlling ecosystem nitrogen cycling in arid and semi-arid grasslands. *Nat. Commun.* **5**, 4799 (2014).
7. J. Yang et al., Amazon drought and forest response: Largely reduced forest photosynthesis but slightly increased canopy greenness during the extreme drought of 2015/2016. *Glob. Change Biol.* **24**, 1919–1934 (2018).
8. N. McDowell et al., Drivers and mechanisms of tree mortality in moist tropical forests. *New Phytol.* **219**, 851–869 (2018).
9. J. D. Brawn, T. J. Benson, M. Stager, N. D. Sly, C. E. Tarwater, Impacts of changing rainfall regime on the demography of tropical birds. *Nat. Clim. Chang.* **7**, 133–136 (2017).
10. T. Hilker et al., Vegetation dynamics and rainfall sensitivity of the Amazon. *Proc. Natl. Acad. Sci. U.S.A.* **111**, 16041–16046 (2014).
11. L. Gibson et al., Primary forests are irreplaceable for sustaining tropical biodiversity. *Nature* **478**, 378–381 (2011).
12. J. Aguirre-Gutiérrez et al., Long-term droughts may drive drier tropical forests towards increased functional, taxonomic and phylogenetic homogeneity. *Nat. Commun.* **11**, 3346 (2020).
13. N. S. Diffenbaugh, C. B. Field, Changes in ecologically critical terrestrial climate conditions. *Science* **341**, 486–492 (2013).
14. S. R. Loarie et al., The velocity of climate change. *Nature* **462**, 1052–1055 (2009).
15. I. Brito-Morales et al., Climate velocity can inform conservation in a warming world. *Trends Ecol. Evol.* **33**, 441–457 (2018).
16. A. Ordonez, J. W. Williams, Projected climate reshuffling based on multivariate climate-availability, climate-analog, and climate-velocity analyses: Implications for community disaggregation. *Clim. Change* **119**, 659–675 (2013).
17. M. T. Burrows et al., Geographical limits to species-range shifts are suggested by climate velocity. *Nature* **507**, 492–495 (2014).
18. I.-C. Chen, J. K. Hill, R. Ohlemüller, D. B. Roy, C. D. Thomas, Rapid range shifts of species associated with high levels of climate warming. *Science* **333**, 1024–1026 (2011).

6 of 7 | PNAS
https://doi.org/10.1073/pnas.2015552118

Shi et al.
Terrestrial biodiversity threatened by increasing global aridity velocity under high-level

19. M. L. Pinsky, B. Worm, M. J. Fogarty, J. L. Sarmiento, S. A. Levin, Marine taxa track local climate velocities. *Science* **341**, 1239–1242 (2013).

20. J. M. Sunday *et al.*, Species traits and climate velocity explain geographic range shifts in an ocean-warming hotspot. *Ecol. Lett.* **18**, 944–953 (2015).

21. Y. Yang, M. L. Roderick, S. Zhang, T. R. McVicar, R. J. Donohue, Hydrologic implications of vegetation response to elevated $CO_2$ in climate projections. *Nat. Clim. Chang.* **9**, 44–48 (2019).

22. W. Zhang *et al.*, Ecosystem structural changes controlled by altered rainfall climatology in tropical savannas. *Nat. Commun.* **10**, 671 (2019).

23. C. R. Schwalm, S. Glendon, P. B. Duffy, RCP8.5 tracks cumulative $CO_2$ emissions. *Proc. Natl. Acad. Sci. U.S.A.* **117**, 19656–19657 (2020).

24. A. Berg, K. A. McColl, No projected global drylands expansion under greenhouse warming. *Nat. Clim. Chang.* **11**, 331–337 (2021).

25. T. F. Keenan, X. Luo, Y. Zhang, S. Zhou, Ecosystem aridity and atmospheric $CO_2$. *Science* **368**, 251–252 (2020).

26. A. M. Ukkola *et al.*, Reduced streamflow in water-stressed climates consistent with $CO2$ effects on vegetation. *Nat. Clim. Chang.* **6**, 75–78 (2016).

27. H. Shimono, H. Nakamura, T. Hasegawa, M. Okada, Lower responsiveness of canopy evapotranspiration rate than of leaf stomatal conductance to open-air $CO2$ elevation in rice. *Glob. Change Biol.* **19**, 2444–2453 (2013).

28. E. Batllori, M.-A. Parisien, S. A. Parks, M. A. Moritz, C. Miller, Potential relocation of climatic environments suggests high rates of climate displacement within the North American protection network. *Glob. Change Biol.* **23**, 3219–3230 (2017).

29. Y. Malhi *et al.*, Climate change, deforestation, and the fate of the Amazon. *Science* **319**, 169–172 (2008).

30. J. Aguirre-Gutiérrez, R. van Treuren, R. Hoekstra, T. J. L. van Hintum, Crop wild relatives range shifts and conservation in Europe under climate change. *Divers. Distrib.* **23**, 739–750 (2017).

31. G. Leng, J. Hall, Crop yield sensitivity of global major agricultural countries to droughts and the projected changes in the future. *Sci. Total Environ.* **654**, 811–821 (2019).

32. L. L. Sloat *et al.*, Climate adaptation by crop migration. *Nat. Commun.* **11**, 1243 (2020).

33. C. Bunn, P. Läderach, O. Ovalle Rivera, D. Kirschke, A bitter cup: Climate change profile of global production of Arabica and Robusta coffee. *Clim. Change* **129**, 89–101 (2015).

34. A. Maxmen, Crop pests: Under attack. *Nature* **501**, S15–S17 (2013).

35. A. F. Taylor, F. E. Kuo, W. C. Sullivan, Views of nature and self-discipline: Evidence from inner city children. *J. Environ. Psychol.* **22**, 49–63 (2002).

36. R. S. Ulrich, View through a window may influence recovery from surgery. *Science* **224**, 420–421 (1984).

37. Y. You, S. Pan, Urban vegetation slows down the spread of coronavirus disease (COVID-19) in the United States. *Geophys. Res. Lett.* **47**, e2020GL089286 (2020).

38. T. P. Dawson, S. T. Jackson, J. I. House, I. C. Prentice, G. M. Mace, Beyond predictions: Biodiversity conservation in a changing climate. *Science* **332**, 53–58 (2011).

39. K. Huang, X. Li, X. Liu, K. C. Seto, Projecting global urban land expansion and heat island intensification through 2050. *Environ. Res. Lett.* **14**, 114037 (2019).

40. E. S. Krayenhoff, A. Moustaoui, A. M. Broadbent, V. Gupta, M. Georgescu, Diurnal interaction between urban expansion, climate change and adaptation in US cities. *Nat. Clim. Chang.* **8**, 1097–1103 (2018).

41. K. W. Oleson, G. B. Bonan, J. Feddema, T. Jackson, An examination of urban heat island characteristics in a global climate model. *Int. J. Climatol.* **31**, 1848–1865 (2011).

42. R. G. Allen, L. S. Pereira, D. Raes, M. Smith, Crop evapotranspiration-Guidelines for computing crop water requirements-FAO Irrigation and drainage paper 56. *FAO, Rome* **300**, D05109 (1998).

43. E. C. Ellis, E. C. Antill, H. Kreft, All is not loss: Plant biodiversity in the anthropocene. *PLoS One* **7**, e30535 (2012).

44. C. N. Jenkins, S. L. Pimm, L. N. Joppa, Global patterns of terrestrial vertebrate diversity and conservation. *Proc. Natl. Acad. Sci. U.S.A.* **110**, E2602–E2610 (2013).

ENVIRONMENTAL SCIENCES

ECOLOGY